Phys. Status Solidi A **208**, No. 10, 2443–2449 (2011) / **DOI** 10.1002/pssa.201026722

physica status solidi pss a
www.pss-a.com
applications and materials science

Bending of nanowire–flexible substrate assemblies integrated via direct synthesis methods

Justin Rodgers, Julia Edel, Johan Rivera, and Ongi Englander*

FAMU-FSU College of Engineering, Florida State University, 2525 Pottsdamer St, Tallahassee, FL 32310, USA

Received 28 November 2010, revised 18 May 2011, accepted 20 May 2011
Published online 17 June 2011

Keywords bending tests, direct integration, flexible substrates, germanium nanowires

* Corresponding author: e-mail englander@eng.fsu.edu, Phone: +1 850 410 6624, Fax: +1 850 410 6337

Nanowires are successfully synthesized directly onto two types of flexible substrates, Kapton and silicone. Reduced temperature catalyst-assisted chemical vapor deposition techniques enable the direct integration. The mechanical properties of these assemblies are evaluated using bending tests where tensile or compressive strains are applied to the samples. Substrate-dependent nanowire properties, thin film formation, and failure of the integrated assemblies are observed.

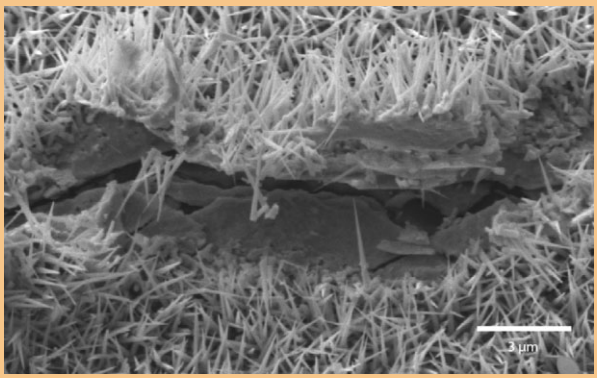

Image: Failure of a germanium nanowire (GeNW) array synthesized on a flexible substrate once subjected to compressive strains.

1 Introduction As interest in flexible electronics and microfluidics has grown over the past decade, polymer and plastic substrates have become commonplace in standard microfabrication processes [1–3]. Such substrates offer many desirable properties including flexibility, bendability, biocompatibility, transparency, and reduced weight. The integration of one-dimensional (1D) nanostructures with flexible substrates to yield flexible and bendable composite assemblies and devices has been widely demonstrated [4–11]. In these examples, individual 1D nanostructures, 1D nanostructure arrays, and 1D nanostructure-based films have been drop cast, transferred by pressing, stamping, or rolling techniques onto a wide range of flexible substrates. The direct integration of bottom-up synthesis mechanisms for 1D nanostructure synthesis with a wide range of substrates is often limited by the high temperature requirements of the catalyst-assisted chemical vapor deposition mechanisms for 1D nanostructure synthesis. Integrated processes which enable nanowire synthesis directly onto thin flexible substrates is of great interest as such approaches eliminate the need to transfer, pick and place nanostructures yet provide basic building blocks for nanoscale applications and devices. We can envision successful integration processes serving as the basis for nanowire-based electrodes for flexible fuel cells, the direct integration of nanowire arrays within microfluidic channels for enhanced flow control or as the basis for manipulating the response of novel metamaterials.

The direct integration of germanium nanowires (GeNWs) with polyimide substrates using reduced temperature vapor–liquid–solid (VLS) techniques has been recently reported [12, 13]. However, the mechanical properties and failure mechanisms of VLS synthesized nanowires–flexible substrate assemblies have yet to be evaluated. The integrity of nanowire-substrate assembly is important in validating the direct integration of bottom-up processes with flexible substrates.

The properties of thin films and thin ribbons on stiff and flexible substrates have been studied in depth [14–21].

Characterization techniques such as bend tests, indentation, MEMS-based testing, and bulge tests are commonly used to evaluate mechanical properties [22–25]. Stress evolution and failure modes are often of interest and may be caused by thermal mismatches, processing stresses, residual stresses, and surface indentation and scratching [14, 17]. With stiff films-flexible substrates combinations, bending causes the substrate to reversibly deform causing the stiff film to crack or debond [16, 17, 26]. Significant efforts have been placed on characterizing electronic devices (thin film transistors and solar cells) fabricated onto flexible substrates and subjected to bending tests [8, 10, 17, 22, 27, 28]. Findings suggest that device performance can be limited by the applied strain but operation of bent devices is possible and in fact, electron mobilities may be enhanced under particular loading conditions [17]. Further, these studies suggest that different devices exhibit different failure modes [27]. Novel mechanics as well as the possibilities offered by flexible substrate-based devices are truly exemplified in these studies.

Here, we report on the direct synthesis of GeNWs onto Kapton and silicone substrates. We also demonstrate that silicon nanowire (SiNW) synthesis directly onto Kapton substrates is possible. We exclusively utilize bottom-up synthesis techniques such that no post synthesis nanowire transfer or manipulation is needed. Next, we characterize the processing results. More specifically, we evaluate fabrication results as a function of substrate, perform bending tests to assess nanowire-substrate adhesion and delamination, and note the role of thin film formation on the resulting assemblies.

2 Experimental methods

2.1 Fabrication Nanowire synthesis follow standard bottom-up processes and takes place in a low pressure chemical vapor deposition (LPCVD) chamber. We select the nanowire synthesis conditions based on robust processes previously established in our lab using standard silicon substrates. Kapton E and silicone are utilized as the flexible substrates in this work and silicon (100) substrates serve as the control substrate. The Kapton substrates are 50 μm-thick, the silicone substrates are 1 mm-thick, and the silicon substrates are 400 μm-thick. According to material specifications, Kapton E can sustain temperatures up to 400 °C and silicone can sustain temperatures up to 315 °C. The substrate selection is motivated by thermal requirements of the nanowire synthesis process. Since to large extent the nanowire synthesis process does not actively involve the substrate (with the exception of the role of pristine single crystalline substrates in controlling the growth direction) a wide range of substrates may be accommodated by the bottom-up synthesis process [29, 30].

The Kapton and silicone samples are cut to size and a sample size of 1 cm by 0.5 cm is used in all experiments. All substrates are first cleaned in acetone and de-ionized (DI) water and dried with a nitrogen gun prior to catalyst application. Thin sputtered gold films are utilized as the bottom-up reaction's catalyst. The silicon substrates are not etched to remove the native oxide as we seek to maintain identical sample preparation steps for all substrates.

GeNW synthesis takes place over a range of process parameters. A temperature of 285 °C and a pressure of 80 Torr using 40 sccm GeH_4 and 100 sccm H_2 is most often used, however multiple parameter combinations in the 270–285 °C temperature range and 7.5–100 Torr pressure range have successfully yielded nanowires. We also demonstrate the integration of SiNWs with Kapton substrates. This synthesis process takes place at 400 °C and 40 Torr using 100 sccm SiH_4 and 100 sccm H_2. For SiNW synthesis, we note that VLS reactions at 440–460 °C yield more desirable results however these temperatures are no longer compatible with the Kapton substrate. Following a 30-min long synthesis process, the furnace is cooled and the samples removed.

To eliminate potential effects of process variations on the synthesis results, for each synthesis process, we simultaneously place a silicon substrate, a Kapton substrate and a silicone substrate within the synthesis chamber (note, silicone is not used for SiNW synthesis). The substrates are placed in close proximity to each other (~0.5 cm between samples) and thus see identical flow conditions. In all cases, the substrates are kept flat during the synthesis process.

2.2 Characterization Mechanical properties of the composite assemblies are examined using bending tests where a bending moment is applied to the sample. The samples are subjected to either tensile or compressive strains. Bending experiments are performed by bending the samples so that the nanowire–substrate interface is strained. Samples are bent to a predetermined radius of curvature (R) as illustrated in Fig. 1 and then allowed to return to the initial position ($R = \infty$). The bending experiments are performed at discrete radii of curvature: 3, 1.5, 1 mm and a hard bend (where the sample folded in half). In all cases, bending takes place along the long axis (1 cm) of the sample. Tensile strain on the assembly is realized by bending to the sample such that nanowires-on-substrate configuration yields a concave down configuration (Fig. 1). Similarly, compressive strain on

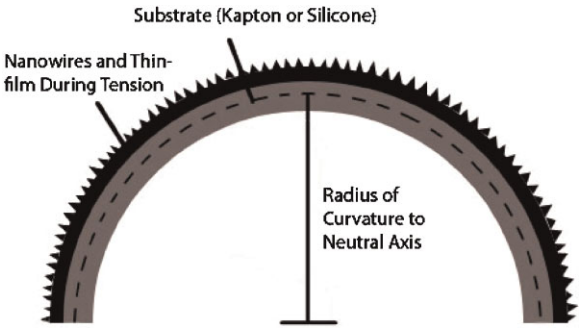

Figure 1 Experimental setup used to apply bending strains onto the samples. The bending experiments are performed at discrete radii of curvature.

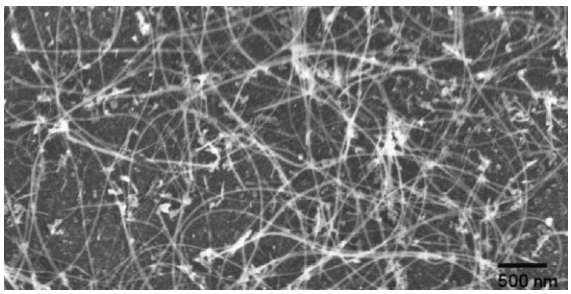

Figure 2 Synthesis results of SiNWs at 400 °C on a Kapton substrate.

the nanowires-on-substrate configuration yields a concave up configuration. The samples are imaged following each bending test using a scanning electron microscope.

3 Results and discussion

3.1 Fabrication results GeNW and SiNW are successfully grown on stiff and flexible substrates under identical synthesis conditions for each material. The flexible substrates consist of Kapton and silicone substrates but the SiNW synthesis is limited to the Kapton substrates due to temperature incompatibilities with the silicone substrate. The SiNWs are of uniform diameter throughout their length (Fig. 2) and we note no observable differences between nanowires synthesized on silicon and on Kapton substrate. The GeNWs exhibit a characteristic taper [Fig. 3(a, b)] [29, 31] on silicon and Kapton substrates while no tapering is observed on the silicone substrate [Fig 3(c)]. With identical gold thin films serving as the reaction catalyst, dense GeNW arrays are obtained, while the SiNW arrays are fairly sparse revealing the substrate. No nanowire alignment or order is noted regardless of substrate.

Images of GeNWs on the various substrates are seen in Fig. 3 and measurements of nanowire growth rates, tip diameter, length, and nanowire density are presented in Table 1. There are no observable differences in nanowire properties (diameter, geometry, nanowire density, and growth rate) for nanowires synthesized on the standard silicon substrate and those synthesized onto the Kapton substrate. The nanowires show a typical taper (thick base and narrow tip) on both substrates and as previously reported [13, 29, 31, 32]. The tapering of GeNWs [Fig. 3(a, b)] is speculated to occur as a result of uncatalyzed germanium deposition onto the growing nanowire. As a result, the base of the nanowire becomes significantly larger than the tip resulting in a cone-shaped nanostructure. The average tip diameter and nanowire density (number of nanowires/μm^2) are almost identical for nanowires synthesized on silicon and Kapton substrates. In both cases, growth rates of $\sim$0.1 μm/min are recorded. Figure 3(c) shows GeNWs on silicone substrates. In this case, we note somewhat different nanowire growth characteristics. Specifically, nanowires with no significant taper, and hence a uniform diameter from base to tip, are observed. The average nanowire diameter is $\sim$58 nm, and considering the standard deviation in measurement, is consistent with nanowire diameters on the silicon and Kapton substrates. This nanowire array, however, is much denser than arrays synthesized on the other substrates. Additionally, a reduced growth rate is observed on the silicone substrates. Ongoing studies are designed to investigate the differences in growth properties. The silicone surface is very rough and we have also observed changes to the surface morphology of the silicone substrate during or following the synthesis process. Specifically, large grain-like sections appear on the surface. We suspect that the silicone

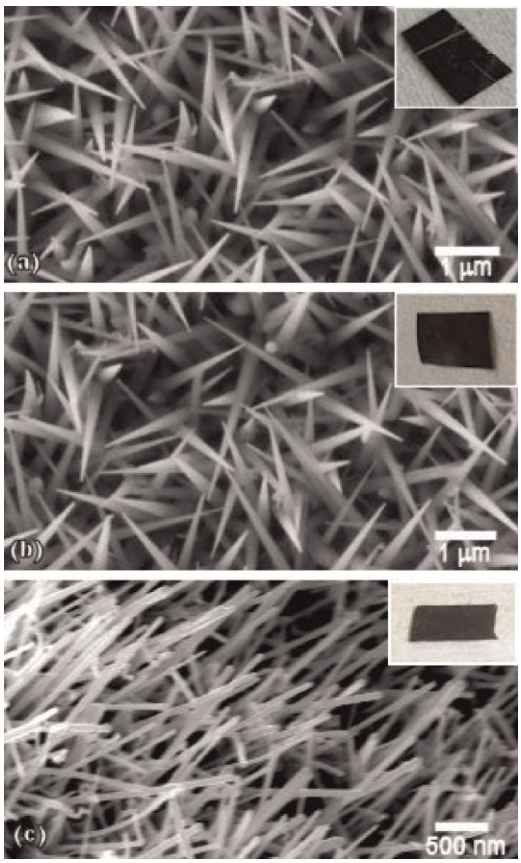

Figure 3 Synthesis of GeNWs at 285 °C. (a) GeNWs on a silicon substrate, (b) GeNWs on a Kapton substrate, and (c) GeNWs on a silicone substrate. Differences in nanowire geometry (tapered *vs.* cylindrical) are observed. Insets present optical images of the samples.

Table 1 GeNW synthesis results.

	GeNWs on silicon	GeNWs on Kapton	GeNWs on silicone
growth rate (μm/min)	0.11 ± 0.02	0.1 ± 0.04	0.05 ± 0.01
tip diameter (nm)	66 ± 12	72 ± 15	58 ± 12
length[a] (μm)	3.4 ± 0.68	3.08 ± 1.1	1.36 ± 0.23
nanowire density (no. of NW/μm^2)	5	6	10

[a]Following a 30-min long synthesis process.

chemistry, which is largely unknown, as well as surface properties, could contribute to these observations. Additionally, the reduced growth rate on silicone substrates could be related to the absence of observable tapering. Optically, GeNWs on silicon and Kapton substrates appear black while GeNWs on the silicone substrates appear dark brown (Fig. 3 insets). We considered the effect of nanowire length (by reducing the nanowire synthesis time) and substrate material on optical response but have found that neither impacts the optical response. Instead, we have observed that tapered nanowire arrays appear black while untapered arrays appear brown.

3.2 Nanowire–substrate interface and thin film formation Next, we investigate the nanowire–substrate interface. To better assess interfacial properties, Focused ion beam (FIB) capabilities are used to uncover the nanowire–substrate interface. Figure 4 illustrates the nanowire–substrate interface for the GeNW-Kapton assembly. The formation of a thin film, while not consistent with the bottom-up synthesis process, has been observed previously in conjunction with the process [13, 32]. We suspect that the thin film formation is due to uncatalyzed germanium deposition onto the side walls of the growing GeNWs which is prevalent at the synthesis temperature. Further, uncatalyzed germanium deposition not only extends the diameter of the nanowires but also fills in regions between the densely growing nanowires forming a germanium thin film. Thus, the formation of the film is consistent with the observed GeNW tapering. In order to avoid FIB related effects and ensure that the apparent continuity of the film is not a result of this processing, or more specifically, the melting of the nanowires during the material removal process we reduce the ion beam energy to 50 pA. We note that the thin film–Kapton interface is smooth, continuous and free of voids and unbonded regions. The Kapton substrate appears to accommodate the deposited film and nanowires well. This thin film formation mechanism does leave behind voids, or incomplete filling, with increasing distance from the interface.

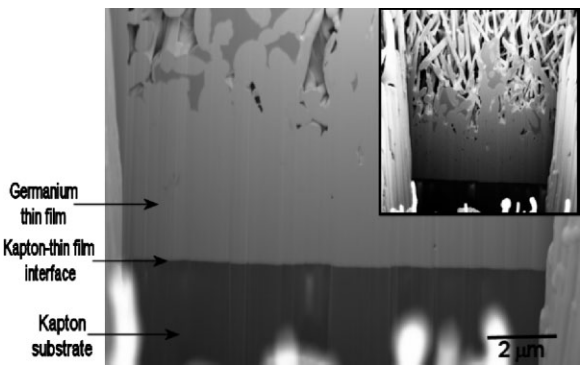

Figure 4 A cross section of the Kapton–GeNW interface generated using FIB capabilities. The Kapton substrate (bottom), the Kapton–thin film interface, the germanium thin film as well as the emergence of individual nanowires (inset) are seen.

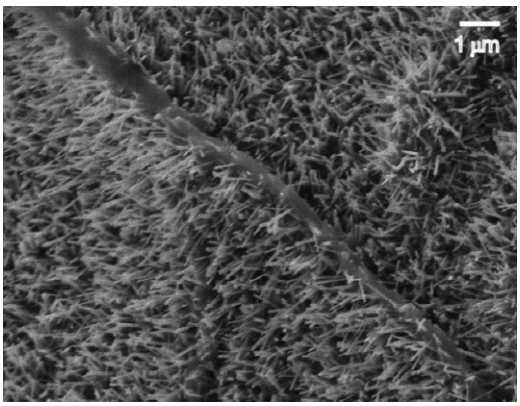

Figure 5 GeNWs on a silicone substrate with a thin film-like structure protruding from within the dense nanowire array.

Eventually, individual nanowires are observed. The film is ~3–4 μm thick but voids in the film are visible within less than 1 μm from the interface. The presence of the voids could contribute to crack formation upon bending as discussed in subsequent sections.

On the silicone samples, thin film formation appears along the surface as seen in Fig. 5. While this behavior is not well understood, we suspect that due to the large difference in the coefficient of thermal expansion of silicone ($\sim 100 \times 10^{-6}$/°C) and germanium (5.8×10^{-6}/°C), the thin film-nanowire array experiences large compressive thermal strains (~10 times larger than thermal strains experienced by the Kapton-GeNW samples) which drive the contraction of the sample upon cooling thus pushing the film away from the surface. The film appears as isolated vertical regions where the nanowire growth is oriented horizontally away from the apparent vertical thin film formation. On these occasions nanowire growth is limited to one edge of the film which is consistent with a structure which is attached to the surface during at least some portion of the synthesis process. Based on the observed solid regions (Fig. 5), the film thickness is estimated to be 0.5–1 μm thick. Unlike the thin film formation on the Kapton substrates, this film formation does not appear to be continuous throughout the surface of the sample. Overall, this analysis points to differences in thin film formation among the two substrates. The substrate along with the resulting nanowire geometry (tapered *vs.* uniform diameter) could have an effect on the thin film formation mechanism and the growth rate.

3.3 Bending test results We have determined that standardized adhesion test methods are not compatible with the samples at hand. Standardized adhesion tests typically rely on an interaction between a known adhesive and a test surface prior to pull and delamination tests. The point contact which would be formed between such an adhesive and nanowire tips greatly reduces the contact area and thus the effectiveness of such test. Therefore, tensile and compressive bending tests are used to analyze failure mechanisms and evaluate allowable strains for each of the composite

assemblies. We have studied multiple samples prepared under identical synthesis conditions. On the Kapton substrates distinct characteristics are observed consistent with thin film failure modes. Under tensile strains, crack behavior showcases channeling characteristics consistent with tensile loads in thin films as illustrated in Fig. 6(a). Generally, a crack begins at a flaw in the thin film and propagates across the film thickness. Once it reaches the surface it elongates laterally and spans the length of sample [14]. While flaws have not been identified within the as-synthesized nanowire arrays, voids noted within the thin film (Fig. 4) could contribute to the observed cracking behavior. Additionally, the proposed thin film formation mechanism is not expected to yield high quality films. We note that cracks originate along the axis of the bend, and additional, parallel cracks are formed away from the central crack extending to the edge of the sample (perpendicular to the bend axis). For the samples studied, tension (or channeling) cracks measure 50–200 nm in width where for each crack, the crack width is rather uniform (within 10 nm) throughout the length of the crack. In compression, a debonding behavior is observed. Debonding is most commonly observed under compressive loading in films with poor adhesion to the surface. Cracks propagate due to unbonded areas that can lead to buckling of the material away from the substrate [Fig. 6(c)]. The presence of parallel cracks, about the bend axis which extend to the edge of the sample (in the direction perpendicular to the bend axis), is observed in compression as well. In tension, a higher crack density is noted and the cracks are in close proximity to each other with an average distance of 5 μm between cracks as illustrated in Fig. 6(a, b). Compressive strains lead to debonding cracks with an average spacing of ~24 μm. While cracks extend to the edge of the sample in the direction perpendicular to the bend axis, the extent of the cracking along to bend axis is a function of the applied strain. The cracking region extends over 100 μm for all samples. The extent of the cracking region in compression is significantly wider (four to nine times) than that in tension and we note wide variations among the samples in this case. A closer examination of the debonding cracks reveals what appears to be the thin film formation between the nanowires and the Kapton substrate as seen in Fig. 6(d). Debonding cracks measure between 800 nm and 4 μm in width. When compared to channeling cracks, debonding cracks are much wider and lack uniformity in width as the crack width varies by as much as 3 μm along its length. As a result, compressive strains appear to yield a more significant perturbation to the nanowire array and the sample as a whole. As seen in Fig. 6(c, d), we note the displacement of the nanowires and the nanowire-thin film combination away from the substrate all along the length of each crack.

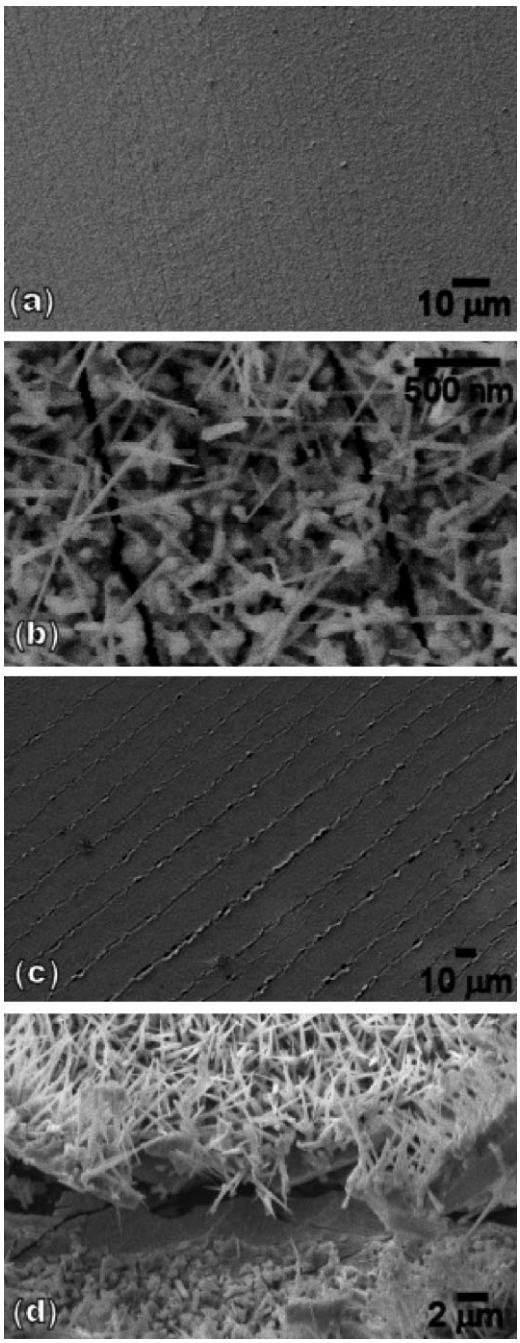

Figure 6 Channeling and debonding behavior of Kapton–GeNW assemblies. (a) Parallel channels form as tensile strain is applied and (b) a close up view of two channels illustrating clean cracks (which appear as dark lines) along the surface. (c) Parallel cracks form as compressive strain is applied. A debonding behavior is noted as material appears to be removed from the surface. (d) A close up view of a debonding crack illustrating nanowires removed from the surface as well as the presence of a film and the Kapton substrate (darkest regions).

The response of the GeNWs-silicone substrate assemblies to strains via bending showcases different characteristics. Overall, the damage to these samples is rather minimal and highly localized. In tension, either no cracks or up to two cracks appear with the onset of bending. Such channeling cracks are seen in Fig. 7. In compression, on the other hand, the samples display no signs of damage or debonding; even when subjected to a hard bend, the surface appears to be undamaged and undisturbed. We note that the nature of these

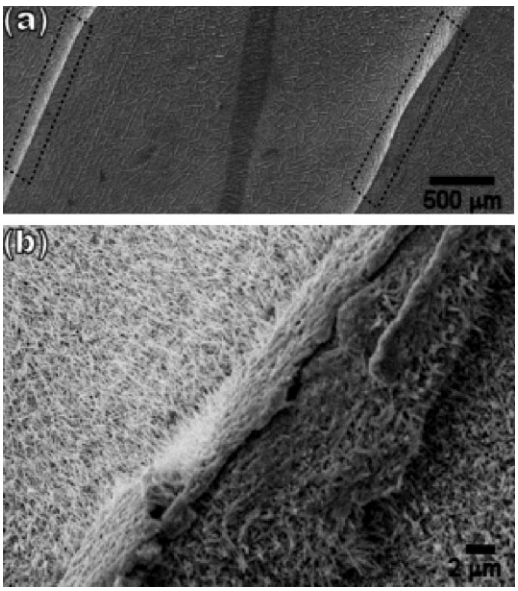

Figure 7 Silicone substrate–GeNWs sample subjected to tensile strain. (a) Two channeling cracks (within dotted boxes) form upon the application of tensile strain. The cracks are distinguishable despite of the sample's rough morphology. (b) A close up view of a channeling crack.

samples and in particular the surface properties of the silicone (Fig. 7) make the analysis of cracking behavior more complex that those of the Kapton based assemblies. We suspect that the nature and final location and orientation of the thin film could affect the samples' response to bending strains. More specifically, the absence of a continuous thin film could prevent traditional failure modes observed on Kapton. Table 2 summarizes the observed results for three sample sets (in each group) evaluated at the largest applied strain values (hard bend). Intermediate strain effects are addressed in subsequent discussion.

3.4 Quantifying strain Film strain (ε) as a function of radius of curvature may be determined using Eq. (1) [26],

Table 2 Summary of cracking behavior under applied strains.

	Kapton substrate	silicone substrate
tensile strain		
distance between cracks (μm)	5 ± 2[a]	none-2500[b]
extent of channeling region (parallel to bend axis) (μm)	145 ± 30[a]	none-2500[b]
number of cracks	18–36[b]	0–2[b]
compressive strain		
distance between cracks (μm)	24 ± 19[a]	none
extent of debonding region (parallel to bend axis) (μm)	780 ± 290[a]	none
number of cracks	18–40[b]	0

[a]Average value plus/minus standard deviation (measurement accuracy ±0.2 μm); [b]range of observed values.

where d is the thickness of the substrate and R is the radius of curvature (applied during the bending test):

$$\varepsilon = d/2R. \quad (1)$$

This relation may be used assuming the thin film is much thinner than its substrate.

Suo and coworkers define various regimes for thin films on flexible substrates which are subjected to bending strains [17, 27]. Specifically, a safe region (no evidence of failure), a transition region and a failure region are all defined as a function of percent strain. We use this approach to map our findings. This analysis includes an observation of four samples in each group, subjected to a sequence of bending tests at $R = 3, 1.5, 1$ mm and a hard bend as well as individual bending tests at each radius. The samples are imaged immediately following each bend test. In this manner we can assess the impact of "pre-existing conditions" on subsequent cracking behavior. With the exception of tensile bending tests on silicone samples, we note consistent behavior within each group of samples and no changes in the onset of failure due to prior bending. The Kapton samples exhibit a safe region in both tension and compression up to a radius of curvature of 1.5 mm or 1.7% strain. Within the safe region there is no evidence of cracking or damage of the nanowire–thin film–substrate structure. Beyond this safe region the samples behave differently depending on the type of strain. A transition region is observed for samples placed in compression within which small cracks appear and a low degree of debonding is observed. This period is followed by pronounced debonding at a radius of curvature of 1 mm or 2.5% strain. We suspect that once the debonding region becomes sufficiently large, film buckling and then fracture takes place [17]. The width of the debonding cracks increases with increasing bending strains. At low strains (transition region), the cracks are initiated but hardly observable. The cracks become wider and displace much material from the surface with increasing strain. Samples subjected to tensile strains exhibit channeling at radii of curvature greater than 1.5 mm or 1.7% strain. The areal extent of the channels and the frequency of the channels increase with increasing strain however, a transition zone prior to failure is not observed.

In comparison, the silicone samples exhibit a different response to the bending tests. Keeping the experimental radii of curvature consistent for the silicone samples and noting that the silicone substrate is 20 times thicker than the Kapton substrate, the silicone samples are subjected to strains 20 times larger. However, the lack of observable cracking, places silicone samples, subjected to compressive strains, within the safe region at all applied strains tested. In tension, we observe two distinct behaviors: either no failure or an immediate failure with the onset of strain with no transition or safe region. Ongoing studies are designed to better understand these observations but the current analysis suggests that the silicone-based assemblies are more tolerant of bending strains.

4 Conclusions We demonstrate the bottom-up synthesis of GeNWs directly onto two types of flexible substrates, Kapton and silicone, yielding integrated assemblies via a single step process. We also observe that it is possible to synthesize SiNWs directly onto Kapton substrates, however, the process renders the Kapton brittle and the assembly fractures easily. This approach is unique as it eliminates complex transfer protocols which are often required to move nanostructures from a stiff donor substrate onto a flexible substrate.

We find that the resulting nanowire properties, the fabricated assemblies' response to applied strains and thin film formation attributes are dependent on the type of flexible substrate used. Nanowire properties are evaluated in terms of nanowire geometry, density, and growth rate and show a notable difference when synthesized on Kapton and silicone substrates under identical synthesis conditions. The mechanical properties of the GeNW–flexible substrate assemblies are evaluated using bending tests and differences in the assemblies' response are observed. The Kapton–GeNW samples illustrate a resistance to failure at up to 2.5% strain in compression while the silicone-GeNW samples show resistance to failure at all levels of applied compressive strain. In tension, the Kapton–GeNW samples are able to withstand 1.7% strain before cracking is observed. The silicone–GeNW samples, on the other hand, may show crack formation when subjected to the smallest amount of tensile strain. With both substrates, the formation of germanium thin films is observed; however, the nature of these films varies with substrate and is suspected to affect bending results.

This study contributes to developing a better understand of the interaction between nanoscale components and compliant substrates. The robustness of the resulting assemblies, their potential failure modes and the overall feasibility of the integration process are all of great importance. Ultimately such studies could provide general and application-specific substrate selection guidelines. Ongoing investigations are designed to better characterize and understand the role of the substrate and its surface properties on the resulting nanowires, the formation of the thin film, and the fabricated assemblies.

Acknowledgements This work was completed with support from Florida State University's start up funds. The authors thank Dr. F. Kametani for assistance with the FIB.

References

[1] S. Roy, J. Phys. D, Appl. Phys. **40**, R413 (2007).
[2] J. Song, H. Jiang, Y. Huang, and J. A. Rogers, J. Vac. Sci. Technol. A **27**, 1107 (2009).
[3] A. C. Siegel, S. T. Phillips, M. D. Dickey, N. Lu, Z. Suo, and G. M. Whitesides, Adv. Funct. Mater. **20**, 28 (2010).
[4] B. Weintraub, Y. L. Deng, and Z. L. Wang, J. Phys. Chem. C **111**, 10162 (2007).
[5] M. C. McAlpine, H. Ahmad, D. Wang, and J. R. Heath, Nature Mater. **6**, 379 (2007).
[6] S. Tawfick, K. O'Brien, and A. J. Hart, Small **5**, 2467 (2009).
[7] T. Y. Tsai, C. Y. Lee, N. H. Tai, and W. H. Tuan, Appl. Phys. Lett. **95**, 013107 (2009).
[8] Z. Fan, H. Razavi, J.-W. Do, A. Moriwaki, O. Ergen, Y.-L. Chueh, P. W. Leu, J. C. Ho, T. Takahashi, L. A. Reichertz, S. Neale, K. Yu, M. Wu, J. W. Ager, and A. Javey, Nature Mater. **8**, 648 (2009).
[9] H. Ko, Z. X. Zhang, J. C. Ho, K. Takei, R. Kapadia, Y. L. Chueh, W. Z. Cao, B. A. Cruden, and A. Javey, Small **6**, 22 (2010).
[10] K. Heo, J. W. Park, J. E. Yang, J. Koh, J. H. Kwon, Y. M. Jhon, M. Kim, M. H. Jo, and S. Hong, Nanotechnology **21**, 6 (2010).
[11] Y. Qi, N. T. Jafferis, K. Lyons, C. M. Lee, H. Ahmad, and M. C. McAlpine, Nano Lett. **10**, 524 (2010).
[12] K. Kang, D. A. Kim, H. S. Lee, C. J. Kim, J. E. Yang, and M. H. Jo, Adv. Mater. **20**, 4684 (2008).
[13] Y. L. Chueh, Z. Y. Fan, K. Takei, H. Ko, R. Kapadia, A. A. Rathore, N. Miller, K. Yu, M. Wu, E. E. Haller, and A. Javey, Nano Lett. **10**, 520 (2010).
[14] K. H. J. Buschow, R. W. Cahn, M. C. Flemings, B. Ilschner, E. J. Kramer, S. Mahajan, and P. Veyssière (eds.), Encyclopedia of Materials: Science and Technology (Elsevier Science, Amsterdam, 2001), p. 3290.
[15] L. B. Freund and S. Suresh, Thin Film Materials: Stress, Defect Formation, and Surface Evolution (Cambridge University Press, New York, 2003).
[16] T. Li, Z. Huang, Z. Suo, S. P. Lacour, and S. Wagner, Appl. Phys. Lett. **85**, 3435 (2004).
[17] G. P. Crawford (ed.), Flexible Flat Panel Displays (Wiley, Chichester, 2005), p. 263.
[18] W. W. Gerberich and M. J. Cordill, Rep. Prog. Phys. **69**, 2157 (2006).
[19] D. Passeri, A. Bettucci, and M. Rossi, Anal. Bioanal. Chem. **396**, 2769 (2010).
[20] S.-I. Park, J.-H. Ahn, X. Feng, S. Wang, Y. Huang, and J. A. Rogers, Adv. Funct. Mater. **18**, 2673 (2008).
[21] J. L. Ni, X. F. Zhu, Z. L. Pei, J. Gong, C. Sun, and P. Zhang, J. Phys. D **42**, 175404 (2009).
[22] H. Gleskova, S. Wagner, and Z. Suo, Appl. Phys. Lett. **75**, 3011 (1999).
[23] B. E. Alaca, J. C. Selby, M. T. A. Saif, and H. Sehitoglu, Rev. Sci. Instrum. **73**, 2963 (2002).
[24] T. Sekitani, Y. Kato, S. Iba, H. Shinaoka, T. Someya, T. Sakurai, and S. Takagi, Appl. Phys. Lett. **86**, (2005).
[25] X. Chen, B. L. Kirsch, R. Senter, S. H. Tolbert, and V. Gupta, Mech. Mater. **41**, 839 (2009).
[26] J. Lewis, Mater. Today **9**, 38 (2006).
[27] H. Gleskova, I.-C. Cheng, S. Wagner, J. C. Sturm, and Z. Suo, Sol. Energy **80**, 687 (2006).
[28] M. Lee, J. Koo, E. A. Chung, D. Y. Jeong, Y. S. Koo, and S. Kim, Nanotechnology **20**, 6 (2009).
[29] H. Adhikari, A. F. Marshall, C. E. D. Chidsey, and P. C. McIntyre, Nano Lett. **6**, 318 (2006).
[30] H. Jagannathan, M. Deal, Y. Nishi, J. Woodruff, C. Chidsey, and P. C. McIntyre, J. Appl. Phys. **100**, 024318 (2006).
[31] D. E. Perea, E. R. Hernesath, E. J. Schwalbach, J. L. Lensch-Falk, P. W. Voorhees, and L. J. Lauhon, Nature Nanotechnol. **4**, 315 (2009).
[32] C.-B. Jin, J.-E. Yang, and M.-H. Jo, Appl. Phys. Lett. **88**, 193105 (2006).